

# PHYS180 Project 3

## Pattern Formation and Biological Application

Owen Morehead, Karoli Clever, Rey Cervantes

April 30, 2021

### 1 Problem 1: Reaction Diffusion and Biological Patterns

Animal coat patterns are one unique result of reaction diffusion systems. Diffusion instabilities drive the mechanism as proposed by Alan Turing in 1952. Turing instabilities occur when the addition of diffusion in a previously homogeneous, steady state makes that system unstable. Consider a system of two substances aka morphogens in reacting and diffusing in embryonic cells. The morphogens are interacting such that for a well-mixed system, there is a spatially uniform steady state (Maini et al., 2012). In a non-mixed system, this steady state is driven unstable by diffusion. These diffusion driven instabilities create the unique and self-organized patterns we see in nature and on animals. This system which Turing studied is described by the following partial differential equation:

$$\frac{\partial \mathbf{u}}{\partial t} = \mathbf{D} \nabla^2 \mathbf{u} + \gamma \mathbf{f}(\mathbf{u}) \quad (1)$$

where  $\mathbf{u}$  is a vector of chemical concentrations,  $\mathbf{D}$  is a matrix of constant diffusion coefficients, and  $\mathbf{f}(\mathbf{u}) = (f(u, v), g(u, v))$  defines the typically nonlinear reaction kinetics. Different boundary and initial conditions can be applied to the system. We consider periodic boundary conditions for the 2D numerical simulation explored. Here we look at a 1D and 2D numerical simulation of a specific reaction diffusion system that is the Thomas system, used to describe common stripe or spot patterns seen on animals:

$$\begin{aligned} f(u, v) &= 150 - u - h(u, v) \\ g(u, v) &= 1.5 \cdot (100 - v) - h(u, v) \\ h(u, v) &= \frac{13uv}{1 + u + u^2/20} \end{aligned} \quad (2)$$

#### 1D

Each step in the discrete numerical implementation consists of diffusing  $\mathbf{u} = (u, v)$ , then adding the reaction function  $\mathbf{f}(\mathbf{u}) = \gamma(f(u, v), g(u, v))$ . The 1D patterns are first seeded with random noise. The array elements which describe the chemical concentrations in space are initially constant but a standard normal distribution of random numbers is added using `numpy.random.standard_normal()`. As the simulation evolves, the pattern develops and becomes evident. We can see from the simulation how the concentration of the chemicals  $u$  and  $v$  varies as a function of  $x$ . In one dimension, what this represents is constant concentration values in one direction or stripes that are displayed over the  $x$  space. Figure 1 shows the final steady state of the one dimensional simulation with  $\gamma = 0.8$ . Starting from an initially random noisy concentration distribution, over time the concentration of these chemicals self-organizes such that the final steady state pattern becomes evident and represents stripes that repeat with a certain frequency over  $x$ .

For  $\gamma = 2.0$ , we see in figure 2 that the frequency of stripes in the steady state increases, meaning the stripes are closer together and more are able to fit in the same size  $x$  space. Changing  $\gamma$  means changing the reaction kinetics by some constant value which in return generates stripes of a certain frequency. A smaller  $\gamma$  means the final steady state will represent stripes that repeat with a lower frequency and larger  $\gamma$  means stripes repeating with a larger frequency.

1D simulation of Turning patterns produced by Thomas system,  $\gamma = 0.8$

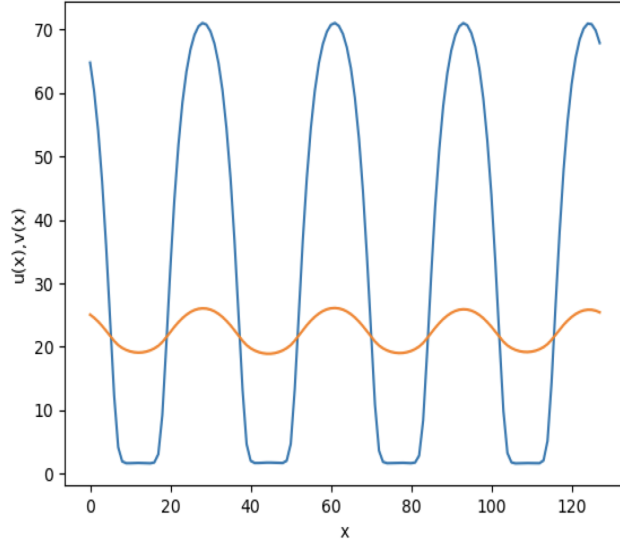


Figure 1: Final steady state of 1D simulation of Thomas system for  $\gamma = 0.8$ . Temporal evolution leads to repeating stripes of a certain frequency.  $u(x)$  is represented in blue,  $v(x)$  in orange.

1D simulation of Turning patterns produced by Thomas system,  $\gamma = 2.0$

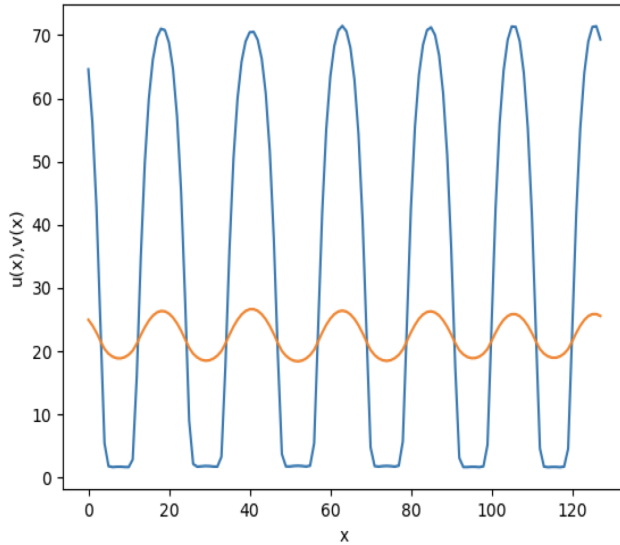


Figure 2: Final steady state of 1D simulation of Thomas system for  $\gamma = 2.0$ . Temporal evolution leads to repeating stripes of a certain frequency. Notice that the frequency of stripes is higher than that from the simulation with  $\gamma = 0.8$ .

The fact that each animal has a unique coat pattern is due to the specific initial conditions set during the embryo stage (Sander, 2001). The patterns developed from these Thomas equations have sensitive dependence on the initial condition, but the characteristics of the patterns depend only on the parameters of the system. This means that each animal has a unique coat pattern yet the global characteristics of the pattern only depend on the species (Sander, 2001). The random noise present in such a developing biological system differs slightly between different individuals within the same species. This is an initial condition

that contributes to the slightly different stripe or spot patterns we see between individuals within the same species.

We can start the 1D numerical pattern by seeding  $u$  and  $v$  with a cosine term of a certain spatial frequency,  $k$ , instead of random noise. The evolution of  $u$  and  $v$  depends on  $k$ . What we find is that there is a band of  $k$  values where the cosine perturbations are unstable, permitting the development of these stripe patterns. Small and large  $k$  values are stable, but for a band of intermediate  $k$  values perturbations will grow exponentially as  $e^{\lambda t}$ , where  $\lambda$ 's are the matrix eigenvalues as described in the analysis done in <https://www.sjsu.edu/faculty/watkins/murray.htm>. This is the solution in time obtained if one solves the 1d differential equation in equation 1 by say separation of variables such that  $u(x, t) = X(x)T(t)$ . The fact that  $\lambda(k) > 0$  for intermediate  $k$  means that  $\lambda(k)$  is a maximum for some non-zero  $k$  in this range. For values of  $k$  in this intermediate band for which the cosine perturbations are unstable, the final pattern is again repeating stripes with a certain frequency. If the system is initialized with a cosine term of a single frequency,  $k$ , the solution will tend to look like  $\cos(kx)$  like we see in the numerical simulation. The frequency of the stripes increases as  $k$  increases. However if  $k$  is too small or large, cosine perturbations are stable and the resulting final steady state is simply a constant  $u$  and  $v$  meaning there are no stripes at all and instead a plain and constant distribution of color.

The results of cosine perturbations tell us that initial small perturbations in density resulting from biological environmental noise can essentially be thought of as a fourier series of cosine terms with certain frequencies. Noise is the random superposition of cosines of different frequencies or  $k$  values.

In thinking about how fast or slow wiggles evolve in time, it makes sense that for perturbations in initial morphogen concentration which are of a very slow frequency aka a long wavelength, big stripe patterns will occur, whereas for a faster frequency concentration perturbation, thin and small stripes will occur. As time goes on, shorter wavelength perturbations will grow and longer wavelengths will shrink down. This means that for small density perturbations, we will see the fastest growing modes of the system.

Since the equations which make up this system are linear for small perturbations, each  $\cos(kx)$  that makes up the random noise can be considered independently of the others. When considering values of  $k$  in the intermediate band, the  $\cos(kx)$  term will be the largest where  $\lambda(k)$  is at its maximum value. As time goes on, the mode with the largest  $\lambda(k)$  will grow the largest in relation to the modes with slower growing  $k$ , those for which  $\lambda(k)$  is smaller.

Overall, what is explored here is that for this system of two different morphogens reacting and diffusing with each other, if we start out with a small amount of noise aka small density perturbations in the morphogens concentrations, the system defined by equation 1 amplifies the noise in certain frequency bands. As time goes on, noise in these certain frequency bands increases in amplitude while noise outside of these frequency bands gets smaller. In 1D, this results in the pattern stripes we see as explored here numerically.

1D simulation of Turning patterns produced by Thomas system,  $\gamma = 0.8$

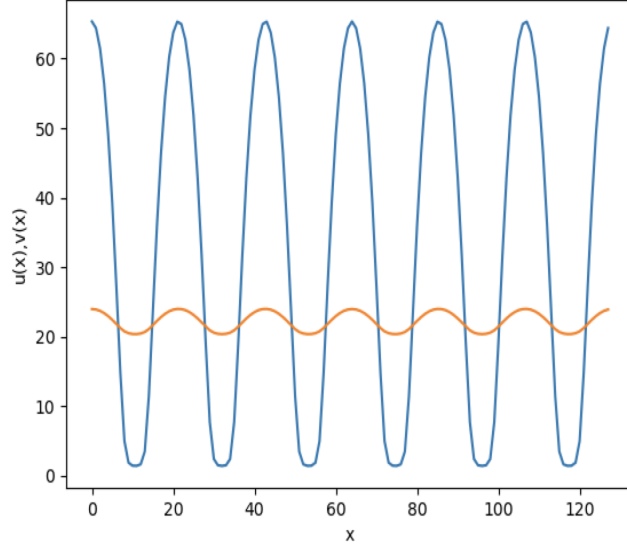


Figure 3: Final steady state of 1D simulation of Thomas system for  $\gamma = 0.8$  and for an initial cosine perturbation,  $\cos(kx)$ , with frequency  $k$ , instead of random noise as in figure 1 and 2. Temporal evolution leads to repeating stripes of a certain frequency. The solution looks like  $\cos(kx)$  for this value of  $k$  = 6 which is inside the band of  $k$  values where  $\lambda(k) > 0$

1D simulation of Turning patterns produced by Thomas system,  $\gamma = 0.8$

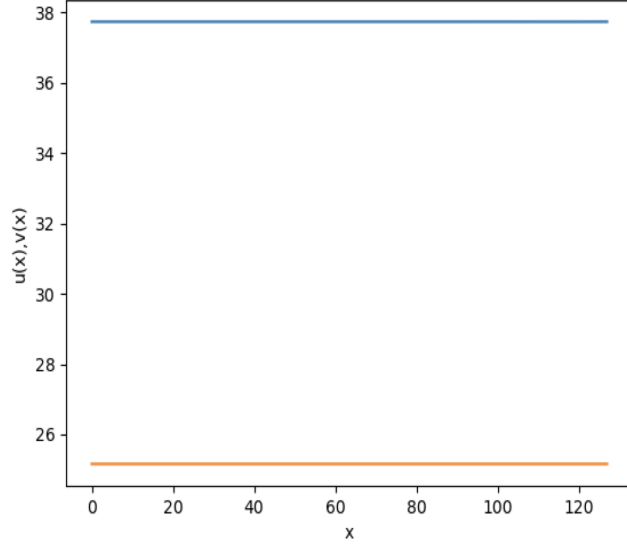


Figure 4: Final steady state of 1D simulation of Thomas system for  $\gamma = 0.8$  and for an initial cosine perturbation,  $\cos(kx)$ , with frequency  $k = 8$ . Because this value of  $k$  is outside the band where  $\lambda(k) > 0$ , the cosine perturbation is stable and temporal evolution leads to constant values of  $u$  and  $v$  such that there is no stripe pattern.

## 2D

Now we examine the numerical simulation of the same reaction-diffusion equation but in 2D. Periodic boundary conditions are applied. This would technically correspond to an animal shaped like a torus or something

that is connected head to tail.

The simulation takes place on a grid which is ( $nx \times ny = 128 \times 128$ ) to start.

Random noise is again added as an initial condition because such a biological system is subject to an internal noisy environment. The initial concentration of morphogens inside the cell is not spatially constant. If it were then no patterns would develop. Fluctuations and noise are at the heart of this pattern formation process.

Through adjusting the parameter  $\gamma$ , it can be seen that for smaller values like  $\gamma = 1.0$ , the final pattern consists of bigger spots and less of them (figure 5). For larger values such as  $\gamma = 10$ , the pattern consists of many more smaller spots (figure 6).

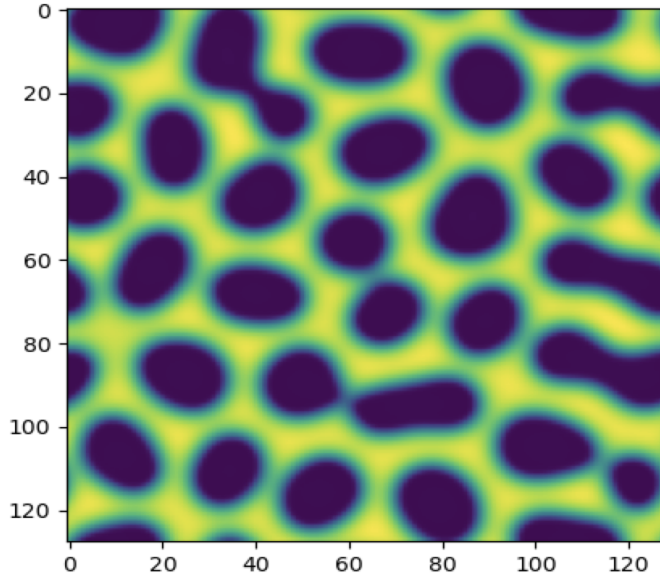


Figure 5: Final steady state of 2D simulation of Thomas system for  $\gamma = 1.0$  with initial random noise. Smaller values of  $\gamma$  such as in this simulation make a pattern that has spots of larger size but less in total.

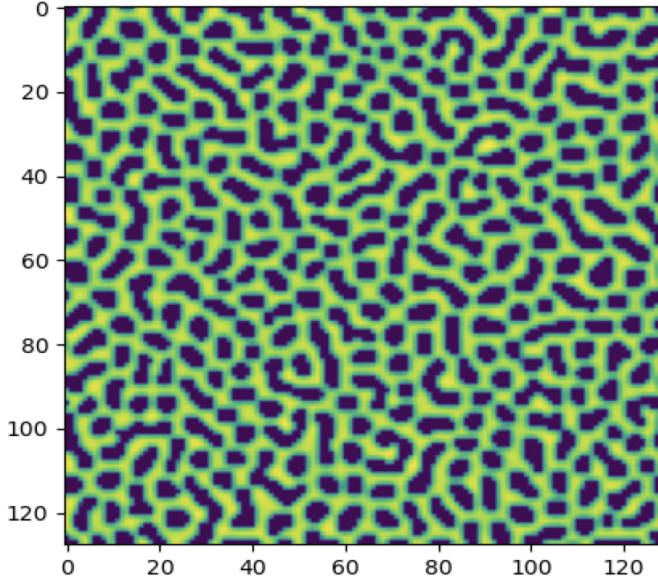


Figure 6: Final steady state of 2D simulation of Thomas system for  $\gamma = 10$  with initial random noise. Larger values of  $\gamma$  such as in this simulation make a pattern that has spots of smaller size and more in total.

If we make one of the dimensions much smaller, for example  $nx = 8$ , such that the shape of this area is more of a narrow rectangle (i.e tail) instead of a larger square (i.e body) we see different pattern dynamics. As seen in figure 7a, if we choose a smaller value of  $\gamma$  say  $\gamma = 1$ , we see the pattern is now stripes. If we choose a larger value say  $\gamma = 6$ , the pattern becomes spotty again with more blob like spots somewhat combined together (figure 7b). Ultimately what is being explored here is the fact that the stripe pattern is favored in narrower geometry. Spots need a larger surface area to form compared to stripes. In a long and narrow area, diffusion is more likely to occur in one direction than the other and this converts the spot pattern into stripes. This is why we see spots on the body of animals such as a jaguar and stripes on their tails. Essentially there is little space for any spots to form on the tail which is why they 'merge' together to form stripes. Analytically we can compare why we get stripes in narrow geometries to the different waveguide modes. Only certain quantized wavevectors,  $k$ , are allowed in a system with certain boundary conditions. When considering boundary conditions that satisfy narrow geometry, the allowed  $k$  values are widely spaced. The perturbations in morphogen concentration grow exponentially as  $e^{\lambda t}$  for unstable eigenvalues,  $\lambda$  in the certain range of  $k$  space. Because the allowed  $k$  values are widely spaced in narrow geometry, these regions in  $k$  space that contain unstable eigenvalues can be easily missed, producing the pattern of stripes and not spots.

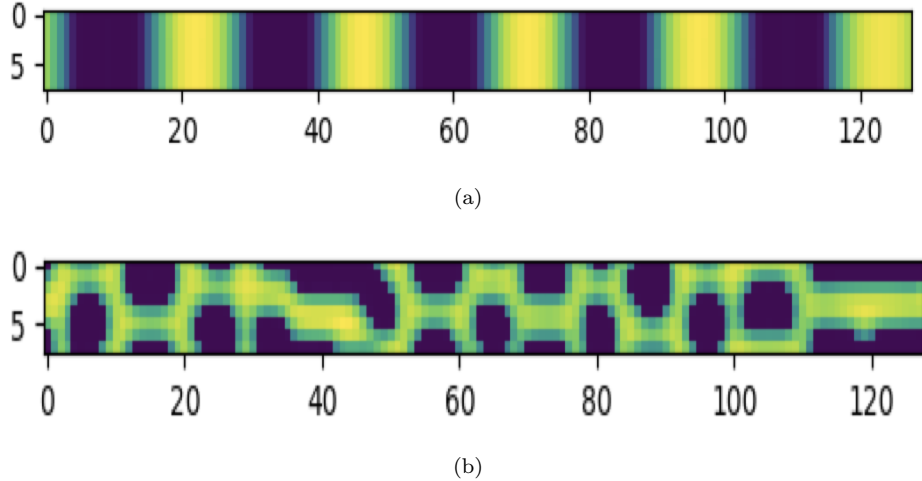


Figure 7: (a) Result of 2D numerical simulation with a grid of size 8x128 and for  $\gamma = 1$ . Resulting pattern is stripes. (b) Result of 2D numerical simulation with a grid of size 8x128 and for  $\gamma = 6$ . Resulting pattern is more spots than stripes but still somewhat of a mix.

Let us now consider the reaction diffusion equations defined by equation 1 such that:

$$\begin{aligned}\frac{\partial u}{\partial t} &= d_1 \cdot \nabla^2 u + \gamma f(u, v) \\ \frac{\partial v}{\partial t} &= d_2 \cdot \nabla^2 v + \gamma g(u, v)\end{aligned}\tag{3}$$

and dividing both sides by  $\gamma$  leads to:

$$\begin{aligned}\frac{1}{\gamma} \frac{\partial u}{\partial t} &= \frac{d_1}{\gamma} \cdot \nabla^2 u + f(u, v) \\ \frac{1}{\gamma} \frac{\partial u}{\partial t} &= \frac{d_2}{\gamma} \cdot \nabla^2 v + g(u, v)\end{aligned}\tag{4}$$

We can understand our findings above and the effects of  $\gamma$  better if we rescale time and space in these equations so that there is no dependence on  $\gamma$ . Consider the following rescaling of time and space:

$$t' = \gamma t \rightarrow \frac{\partial u}{\partial t'} = \frac{dt}{dt'} \frac{\partial u}{\partial t} = \frac{1}{\gamma} \frac{\partial u}{\partial t}\tag{5}$$

and,

$$r' = \sqrt{\gamma} r \rightarrow \nabla^2 u = \gamma \nabla'^2 u.\tag{6}$$

This leads to the system of equations:

$$\begin{aligned}\frac{\partial u}{\partial t'} &= d_1 \cdot \nabla'^2 u' + f(u, v) \\ \frac{\partial v}{\partial t'} &= d_2 \cdot \nabla'^2 v' + g(u, v)\end{aligned}\tag{7}$$

From this we can better understand the effects of gamma. We see from equation 5 that increasing  $\gamma$  has the effect of increasing the timestep,  $dt$ , of the simulation, making it run faster. We can also see this if we consider the solution to a simplified homogeneous version of the reaction diffusion equation such that  $u(x, t) = T(t)X(x) = e^{k\gamma t} \sin(\sqrt{\frac{k\lambda}{d}} x)$ . If we consider  $t' = \gamma t$  and  $x' = \sqrt{\gamma} x$ , we can see how this rescaling

effects the solution. In terms of the variable  $t$ ,  $e^{k\gamma t} = e^{kt'}$  and a larger value of  $\gamma$  is going to make the time evolution speed up.

In terms of the variable  $x$ ,  $\sin(\sqrt{\frac{k\lambda}{d}}x) = \sin(\sqrt{\frac{k}{d}}kx')$  and so the spacing of the sinusoidal function is going to decrease as  $\gamma$  increases. The spacing between zeros is  $\pi$ ,  $\rightarrow$  for  $x' = 0$  and  $\sqrt{k/d}x' = \pi$ ,  $X(x) = 0$ . Equivalently for  $\sqrt{\gamma}x = 0$  and  $\sqrt{k/d}\sqrt{\gamma}x = \pi$ ,  $X(x) = 0$ . From this we can see that  $X(x) = 0$  for  $x = 0$  and  $x = \pi\sqrt{d}/\sqrt{\gamma k}$ . This means that the spacing between zeros is  $\pi\sqrt{d}/\sqrt{\gamma k}$ . So for larger values of  $\gamma$ , the spacing between zeros is going to be smaller. For smaller  $\gamma$ , the spacing between zeros is going to be larger (spacing  $\propto 1/\sqrt{\gamma}$ ). We can also see that the spacing between zeros otherwise said the spacing between spots in the pattern is also proportional to the diffusion coefficient such that spacing  $\propto \sqrt{d}$ . These diffusion coefficients also contribute to whether or not the spot pattern consist of smaller spots that are closer together or larger spots that are farther apart.

In summary we see that for larger  $\gamma$ , the simulation will evolve faster i.e. time is contracted and the average spacing between spots in the pattern will be smaller i.e the patterns in the x-y plane will be contracted. For smaller  $\gamma$ , the simulation time is diluted or slower and the average spacing between spots in the pattern will be larger, resulting in larger spots that are more spaced out.

## Biological Relevance of these Models

Alan Turing's reaction-diffusion model uses a two-protein system which generates a pattern of evenly spaced spots. This pattern can further be converted to stripes when including a third external force. The model requires that there is one activating protein, activating itself plus an inhibitory protein, which in turn only inhibits the activator. The activating protein transient expression by itself would only produce a pattern of both proteins off or spot of inhibitor on, because the activator would activate the inhibitor, hence turning the expression of activator off. When the molecules diffuse or are transported across the tissue, the activator gets randomly turned on, diffusing away from its point source, and thereby activating itself in any nearby cells. Yet simultaneously will activate the inhibitor, which also diffuses away from the point source, thus inhibiting the activator. Depending on the timing, activation, diffusion or transport, this results in the formation of an expanding ring of activator expression. For spots, though, we need random fluctuations in expression which will turn the activator on at low levels across a specific tissue. Furthermore, to get spots, the activator has to diffuse slower than the inhibitor, and here, random spots of activator can stabilize as soon as they are far enough apart from one another (Rivera, A., 2021). These small spots will activate the expression of a slowly diffusing activator, as well as a quickly diffusing inhibitor, and the gradient will prevent any nearby cells from making the activator, which gives us the fairly regular pattern. This pattern depends on size and shape of the tissue, as well as the speed of the activator/inhibitor diffusion. Other pattern elements might be present depending on further pattern elements. When dealing with long and narrow tissues, diffusion can occur only in one direction, which gives the stripe pattern. But directional growth or morphogenic gradient can convert spots to stripes as well. When an external force is missing, spots or a labyrinth pattern is expected depending on activator/inhibitor properties. But other ideas have been proposed such as making diffusion more likely in one direction. The tissue would then be subject to a production gradient, which can be a protein or other cofactor such as transcriptional or translational, resulting in higher gene expression of activator/inhibitor on only one side of the tissue. In models, this would relate to stripes that are orthogonal to the gradient. When there is a parameter gradient, these stripes will run parallel to it, meaning that the activation and inhibition properties of proteins will be more present at one end of the tissue. Furthermore, the tissue can grow directionally, such as limbs growing away from a body, caused by cell proliferations underneath the limb bud. The rate of growth will be slower in other directions of that particular limb (Rivera, A., 2021).

Some biological examples of where the same general mechanisms proposed by Turing are thought to be used are for example the patterns in cows or zebras. We can also look at such mammals as the leopard or tiger. Sea creatures also display this types of mechanisms for example a diversity of mollusks and sea snails. Each of these animals from a diversity of species has it's very unique pattern yet the type of pattern is the same across the species. The patterns dependent on initial conditions, yet size and shape of patterns are only dependent on parameters of the system. Color changes such as in octopodi or chameleons are due to a different



Figure 8: (a) Shown the flower-like pattern of a jaguar in (a.a), and the computer generated analogous pattern of a jaguar (a.b) produced by two coupled activator-inhibitor processes (Ball, P., 2015). (b) The expected striped pattern of a tiger, individually unique to each specimen, yet the same across the species (Quanta Magazine, 2013).

kind of mechanism. They have specialized cells in their skin called chromatophores. Each chromatophore cell has a stretchy sac, the cyto-elastic sacculus, which is filled with pigment. This pigment can be red, yellow, brown or black. The muscles around the cell tighten and pull the pigment sac wider, which allows for more pigment to be visible. When the muscles relax, the pigment sac shrinks in size and let less pigment be visible. Cephalopod/Octopodi or Squid chromatophores are unique compared to other chromatophores in the animal kingdom. Each chromatophore cell is attached to a nerve, meaning the expansion or contraction of the cells is controlled by the nervous system. When the animal sees something, like a predator or prey, that prompts it to change color, its brain sends a signal to the chromatophores (Ocean Conservancy, 2019). Therefore, this type of color and pattern change is a successful different kind of mechanism compared to the Turing model.

Other mechanisms that have been found to produce the complex structures and functions found in organisms are such as the chemical reaction by Belousov-Zhabotinsky, containing Sodium Bromate, Sulfuric Acid, Sodium Bromide, Malonic Acid, Ferroin, and Water. The chemicals are mixed carefully where proper

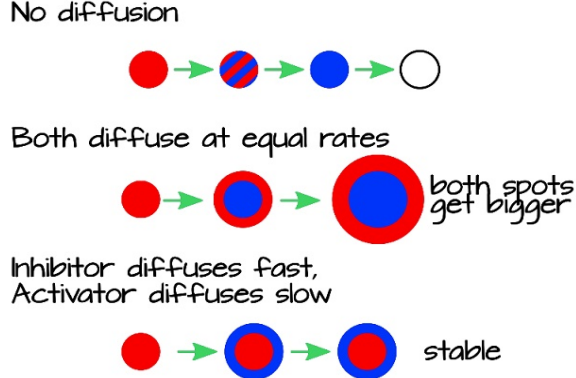


Figure 9: Turing pattern with activator shown in red and inhibitor shown in blue. The activator activates itself and the inhibitor, and the inhibitor only inhibits the activator, yet if the inhibitor diffuses more quickly than the activator, it will result in a regular pattern of spots (Rivera, A., 2021).

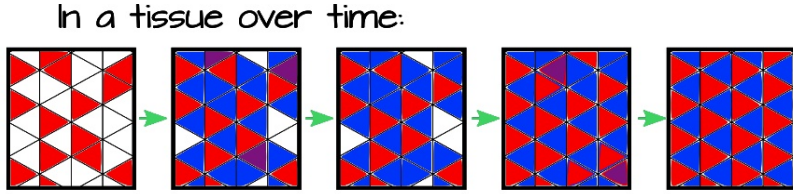


Figure 10: Shown here the activator is randomly expressed at low levels in a subset of cells over a tissue. It self-activates to increase its own expression levels while also activating the inhibitor (panel 1). The inhibitor quickly diffuses to the adjacent cells (second panel). Cells with both activator and inhibitor (purple) quickly convert to inhibitor-only as the inhibitor turns the activator off (third panel). Cells that are not exposed to the inhibitor (white) can randomly turn on the activator, turning on the diffusible inhibitor (fourth panel). This quickly sets up a stable pattern of on-mode and off-mode in cells (fifth panel) (Rivera, A., 2021).

handling and ratio are of utmost importance to successfully create a reaction that will show a pattern of waves radiating out from random points in the liquid. The reaction will go on for several minutes depending on the volume, until some state of reaction equilibrium is reached (Barzykina, I., 2020).

A further example is that of fractals, which are shapes made of parts that are very similar to the whole such as the fancy Romanesco broccoli. Other self-similar morphology patterns use a methodology of scale invariance. such as the Mandelbrot sets, Julia sets, a Sierpinski gasket, or Sierpinski carpet which is also generated by a fractal tree. Additional forms of fractals are sounds, circadian rhythms, slime molds, and digital computer imaging called in-silico modeling (Wikipedia.org, 2021).

Creations of complex structures in biology differ from those made by human technology through evolution and environment, often genetics, constant change of ecosystems, supply and demand. Code is static and needs pre-meditated input, although we can program some random factors, but they are still pre-meditated. Evelyn Sander gives an example of a cow and its clone having different spots, even though the same genetics. This is because the pattern of the spots on the particular cow are determined by the environment in the embryonic state. Some advantages in Turing's mechanism are the controlled mathematical inclusion of diffusion and the ability to vary this in theoretical applications. Disadvantages are perhaps limitations between stripes and spots only being one-directional and not technically being able to appear on the same animal, although it has been observed that common house cats, such as tabbies that have stripes, and spots. Mechanisms such as fractals or Fibonacci sets found in nature show that lifeforms tend to repeat physiology that is of benefit and advantageous to the organism, which would be dependent on biological and ecological influences which the Turing model cannot necessarily include thus far.

Plants often show self-similar morphology and some examples of this would be found in the example of fancy Romanesco broccoli, leaf veining, aquatic plants such as the elodea, branching root systems, spruce trees,

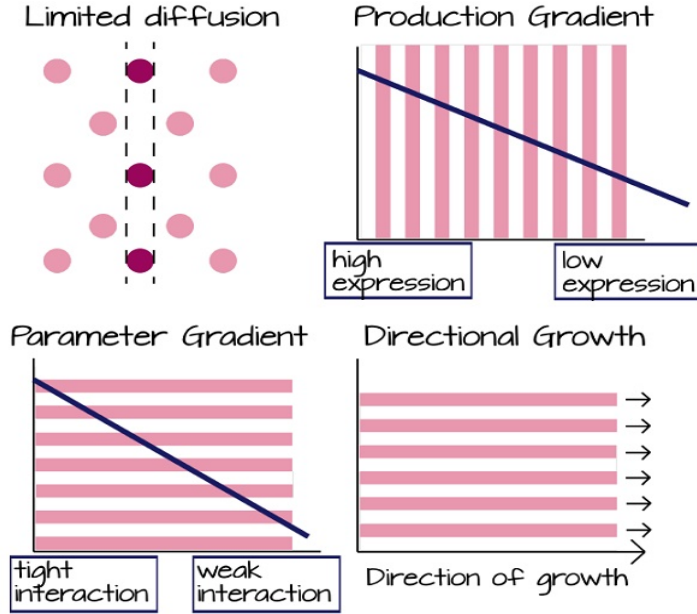


Figure 11: Directional growth and morphogenic gradient will convert the spot pattern into stripes (Rivera, A., 2021).



Figure 12: Patterns found on seashells and the corresponding analogues in activator-inhibitor systems (Ball, P., 2015).

ferns, and whorl patterns of woodruff. In mammals we can see such patterns in vascular, lung, or tracheal tissues which branch the same self-similar fashion (Deutsch, J., 2021).

A viable theory for how such self-similar structures are produced would be the success of the structure and genetic evolution after environmental influences favored certain shapes. We can further use an example of bacteria finding random walking food such as glucose which will direct the branching bacterial growth to be present in the direction of the food. This will create a branching pattern as the food source randomly reaches it and is immediately dependent on reaction to the environment. There would be no mathematical reasoning that could be easily formulated, since this is highly dependent on quantity, quality and type of food source (Deutsch, J., 2021). Tree tops and their branching patterns bring to mind the necessity for photosynthesis, and how each branch needs to fan out to get optimal exposure, therefore the individual smaller branches will follow a repetitive specific pattern to thrive. The environment driven needs will replicate successful patterns,



Figure 13: Petri dish with chemical reaction showing the Belousov-Zhabotinsky model for pattern formation (Ball, P., 2015).



Figure 14: Chameleon with color cells that are activated via neurons and not Turing model pattern (Quanta Magazine, 2013).

and eliminate those that don't work, or as an alternative, the organism will need to attract some form of symbiotic partnership. Chemical reactions are dependent on what materials are available, yet can cause pattern formation and self-similar structures such as crystals and condensations (Wikipedia.org, 2021).



Figure 15: Fibonacci series in flowers is shown on the left with a different mathematical and genetic method of pattern formation as well as fancy broccoli fractal pattern shown on the right, where each unit is a repeat in form and shape of the whole (Ball, P., 2015).

## 2 Problem 3: Origins of Dendritic Growth

### Dendritic Growth

This next problem explores pattern formation as it occurs with the growth of a boundary surface between two phases. With the diffusion of a specific quantity (such as latent heat) on this interface, instability grows and leads to undulations, which contort the boundary and lead to the formation of patterns. This method is shown as dendritic (tree-like) growth, and a well-studied example of this is the formation of the snowflake. Considering the snowflake, the two competing domains are ice and water, where an ice crystal is immersed in super-cooled liquid water (below the freezing point of water), and where the growth comes from the ice crystal nucleus. The growth rate is limited by the diffusion of latent heat, and the pattern growth is controlled by external aspects of the environment (such as temperature and humidity). Combined with the crystalline anisotropy, these elements create the dendritic branches of the snowflake, which are practically identical to each other. Snowflakes receive their unique patterns due to even tiny changes in those elements producing significant changes in growth patterns. Contrasting with pattern formations of biological entities, that have genetic influence, there is no pre-existing road-map for the snowflake pattern or internal coordinator managing the growth of a specific pattern. Thus, aesthetically pleasing iterations of snowflake patterns we can see are nature's own works of art. The following scripts utilize the phase model of the system in order to simulate dendritic growth, and it is important to note that it deals with simple physical systems such as that between ice and water (such as the snowflake), rather than dendritic growth in biological systems. In this case, the diffusion of latent heat is particularly notable. As shown in the equation below, the flow of heat  $\mathbf{J}$  is proportional to the negative gradient of temperature.

$$\begin{aligned}\mathbf{J} &= -D\nabla T \\ \mathbf{J} &\propto -\nabla T\end{aligned}\tag{8}$$

Also, the reason it is possible to simulate the process of ice and super-cooled water is due to the ice being curved. This lowers the equilibrium temperature needed to freeze liquid water, moving it down from 0 degrees Celsius to a value of  $-\frac{C}{R}$ , where  $C$  is a constant and  $R$  is the radius of the curvature.

Running `dend.py`, the central nucleation site displays dendritic growth, with four-fold symmetry, with

four quadrants displaying the same growth pattern. Figure 16 below displays the output after letting the simulation run for a few minutes.

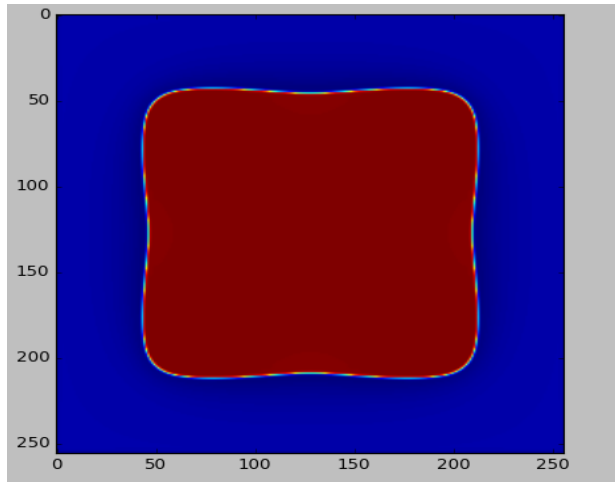


Figure 16: Displays the dend.py simulation, where the red area represents the growing ice crystal structure and the blue area represents the super-cooled water body. As can be seen, there is four-fold symmetry in the product. Such is the process of the formation of the "snowflake."

In order to speed up this computation, we can run `quart_dend.py`, which reflects one of the four quadrants (the other three would be the same due to the symmetry). Figure 17 below displays the output after letting it run for a minute and thirty seconds.

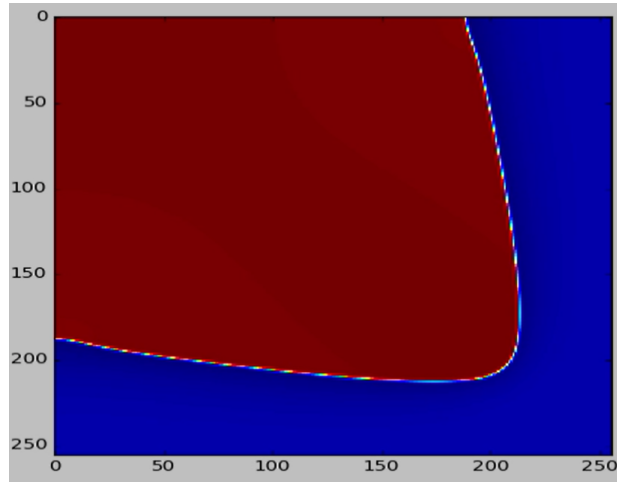


Figure 17: Displays the `quart_dend.py` simulation, which is the bottom right quadrant of the `dend.py` simulation. The computation is much faster, which the tip of the ice formation approaching the lower right limit quicker than using the `dend.py` code.

Looking at the quart\_dend.py code, the model has a similar diffusion equation as to the diffusion equation studying the spots on coats of animals, but it has two diffusion or diffusion-like terms. The first is the diffusion of temperature, which dictates if it will be ice or water. The second term is shown in  $\phi$ , which represents the phase field or the “diffusion” of the ice phase. With the continuous variable having two stable values, such as (-1) for ice and (1) for water, it can be modelled in a continuous process, where the stability depends on the temperature. In the case that the temperature is zero, there will be two stable situations in both ice and water. In the case of a higher temperature, the liquid phase becomes more stable, and the ice phase becomes metastable. In the case of a lower temperature, it is the opposite, where the ice phase becomes more stable, and the water phase becomes metastable. It is this combination of diffusion-like terms that determine it to be more stable as ice or water depending on the temperature.

In quart\_dend.py, there were commented lines that varied the anisotropy. The default presented to us was the anisotropic “diffusion” of the  $\phi$  field or diffusion of the ice phase, and the results were shown earlier in Figure 17. The following Figures display the outputs of the other cases—where there was anisotropic “diffusion” in another direction (Figure 18), a diffusion that is much more anisotropic (Figure 19), and an almost isotropic diffusion of the  $\phi$  field (Figure 20).

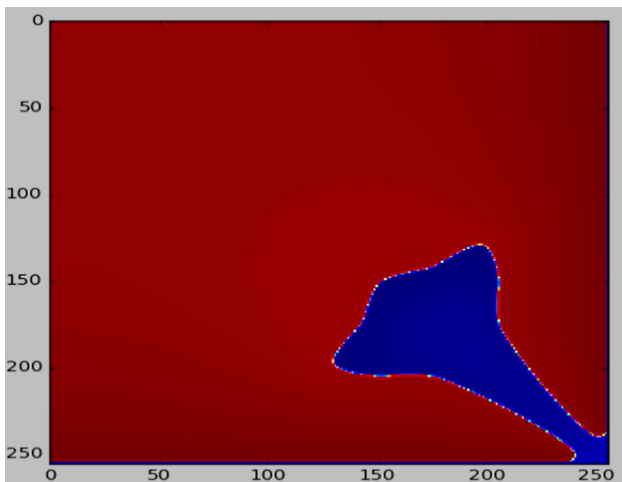


Figure 18: Displays the case of anisotropic ”diffusion” in another direction. The following values changed:  $c_1$  went from 0.25 to 0.1,  $c_2$  went from -0.0 to 0.15, and  $\epsilon$ s went from 0.5 to 0.75. The time elapsed was about 9 minutes.

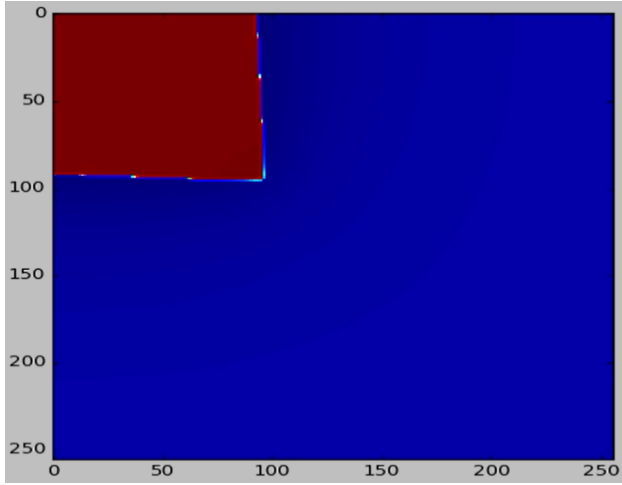


Figure 19: Displays the case of a much more anisotropic "diffusion." Here the following values changed:  $c_1$  went from 0.25 to 0.35, and  $c_2$  went from -0.0 to -0.1. There was no change in  $\epsilon$ . The time elapsed was about 3.5 minutes.

It is in the fourth case, where there is almost an isotropic diffusion of the phi field, it is very difficult to see any dendritic instability. What this suggests is that there must be a presence of interfacial anisotropy in order to simulate dendrites and create dendrite arms.

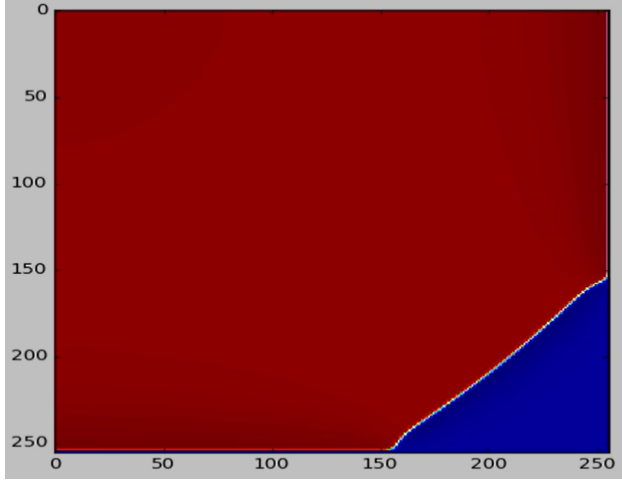


Figure 20: Displays the case of an almost isotropic "diffusion" of the ice phase  $\phi$ . The following values changed:  $c_1$  went from 0.25 to  $C_1(0.17)$ , and  $c_2$  went from -0.0 to  $C_2(0.08)$ . There was no change in  $\epsilon$ . The time elapsed was about 1.5 minutes.

### Mullins-Sekerka Instability

This following topic revolves around the Mullins-Sekerka mechanism, which results in the interfacial instability that, in the case of solidification (such as the snowflake example), runs the process of pattern formation. This instability is related to both dendritic growth and to the fractal nature of Diffusion Limited Aggregation (DLA), as the model displays a surface of ice that moves to the right into a large body of super-cooled water. The reason that it does not freeze instantaneously is due to the diffusion of latent heat from the surface of the ice before more of the super-cooled water can freeze. The analogy provided in the homework description compares the diffusion of heat to the diffusion of a particle, where "cooling" particles hit the surface of the ice and can diffuse the latent heat, allowing the ice to grow.

Running `mul_suk.py`, without any changes to the code, produces Figure 21 below.

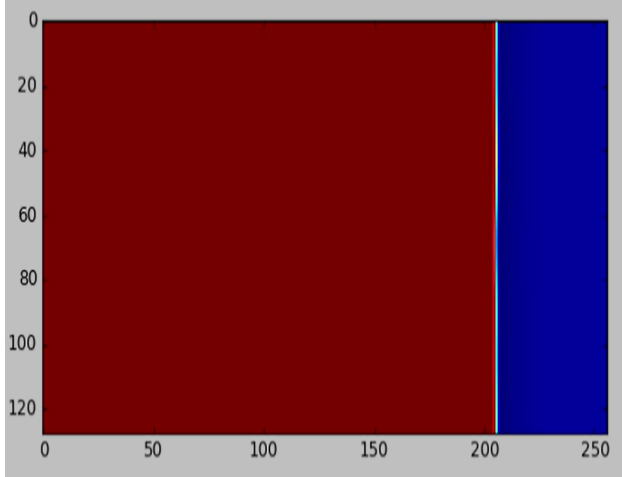


Figure 21: The output when running the `mul_suk.py` simulation. There were small undulations in the beginning, until about  $ny = 75$ , where the surface flattened out.

In order to test what occurs as the vertical height changes as well as the frequency, we will take trials with varying  $nx$  and different integral multiples of the lowest mode of frequency. The default code had a vertical height (period of oscillation) of  $nx = 128$ , and the frequency multiplied by 3. Figure 22 shows the output when  $nx = 64$ , or half of the original vertical height, as well as the output when  $nx = 256$ , or double of the original vertical height.

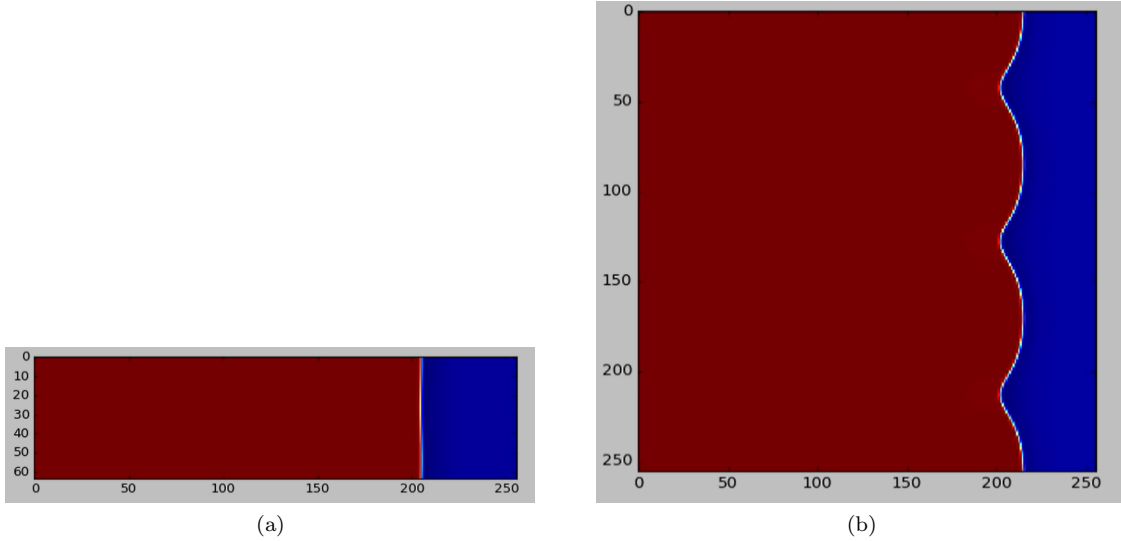


Figure 22: (a) The output of running  $nx = 64$  with 3 times the frequency. In this instance, the small undulations in the beginning faded at around  $ny = 30$ . (b) The output of running  $nx = 256$  with 3 times the frequency. Here, the undulations remained, with the peaks growing more rapidly compared to the troughs.

Next, we viewed the results from with the lowest mode of frequency (multiplied by 1). Figure 23 shows this result with  $nx = 64$  (a),  $nx = 128$  (b), and  $nx = 256$  (c).

Then we try multiplying the frequency by 2, while again testing for  $nx = 64$ ,  $nx = 128$ , and  $nx = 256$ . These are shown in Figure 24, (a), (b) and (c) respectively.

Finally, we'll have the frequency multiplied by 4. Again, we will test  $nx = 64$ ,  $nx = 128$ , and  $nx = 256$ . These are shown in Figure 25, (a), (b) and (c) respectively.

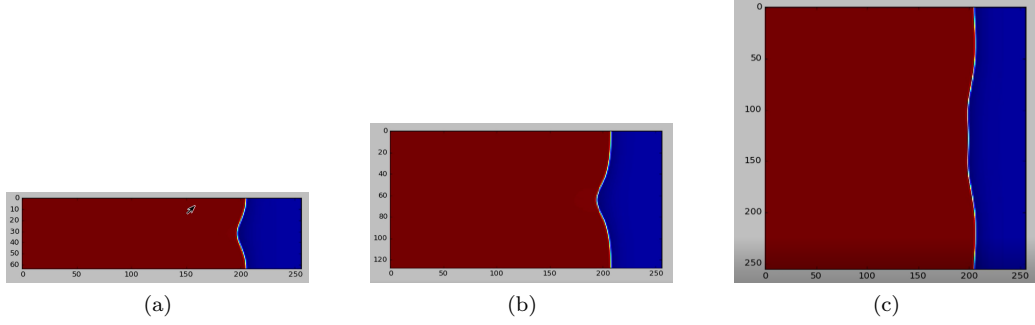


Figure 23: (a) The output of running  $nx = 64$  with the frequency multiplied by 1. Here the undulations result in peaks at the top and bottom of the screen with one deep trough in the center. (b) The output of running  $nx = 128$  with the frequency multiplied by 1. Similarly, there are two peaks at the top and bottom, and a trough in the center, though it is not as drastically deep. (c) The output of running  $nx = 256$  with the frequency multiplied by 1. Here, the peaks have leveled considerably more and the trough is not deep.

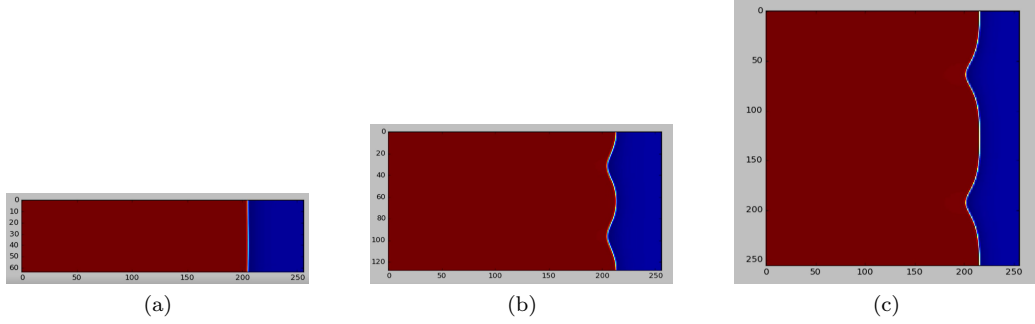


Figure 24: (a) The output of running  $nx = 64$  with the frequency multiplied by 2. Here, the undulations were present up until about  $ny = 35$ . (b) The output of running  $nx = 128$  with the frequency multiplied by 2. Here, there are three peaks and two troughs. (c) The output of running  $nx = 256$  with the frequency multiplied by 2. Here, The figure is much more bloated, with less of a difference in growth between the troughs and the peaks compared to (b).

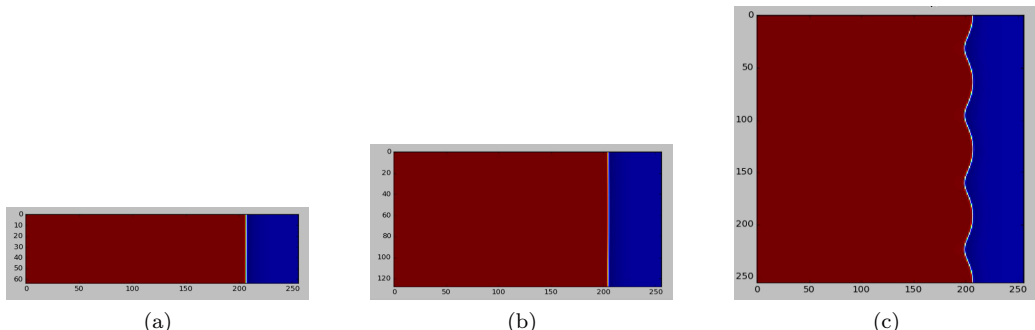


Figure 25: (a) The output of running  $nx = 64$  with the frequency multiplied by 4. Here, the undulations were present up until about  $ny = 15$  before it flattened out. (b) The output of running  $nx = 128$  with the frequency multiplied by 4. Here, the undulations were present up until about  $ny = 50$  before it flattened. (c) The output of running  $nx = 256$  with the frequency multiplied by 4. There are five peaks and four troughs.

To better understand the process of the Mullins-Sekerka instability, we can consider a steady-state interface that experiences perturbations.

$$\zeta(x, t) = \xi_k * \exp(ik * x + \omega_k t) \quad (9)$$

Here,  $k$  is a 2-dimensional wave vector perpendicular to velocity and  $\omega_k$  is the amplification rate that determines stability based on its sign. Should it be positive, the undulations will increase and should it be negative, the undulations will decrease. An equation for  $\omega_k$  can be found, such that it is proportional to  $k(1 - Ak^2)$ , noted in formula 3.14 in Langer's Review of (Non-Biological) Dendrites, included below:

$$\omega_k = kv[1 - \frac{1}{2}(1 + \beta)d_0lk^2] \quad (10)$$

The first part of the equation above is a positive, destabilizing term that scales to the velocity and the second is a negative, stabilizing term that hold the surface tension. At small values of  $k$ , the expression for  $\omega_k$  is positive and there is instability, allowing for exponential growth. At larger values of  $k$ , however, the opposite is true. At significantly large  $k$  values,  $\omega_k$  becomes negative and thus the system undulates very slowly due to it being stable.

It is neat to note that the pattern formations observed in Figure 23(a), Figure 24 (b), and Figure 25 (c) are the same! This is due to them having the same frequency, simplifying to  $2\pi/64$  after the proper  $nx$  and integer multiples were applied. Generally, as the frequency increased we saw the presence of more undulations that sustained growth. With undulations with significant peaks, latent heat is able to diffuse much more quickly. With this high curvature, it can meet the field lines and thus allow the heat to escape faster compared to the troughs or a flat surface.

## Relationship to Biological Systems that Exhibit a Branching Morphology

Instability similar to the Mullins-Sekerka can be found in Zwicker et al. research, examining the behavior of droplets in systems which are maintained away from thermodynamic equilibrium through external supply of energy. Droplets are grown through the addition of droplet material generated by chemical reactions. This chemically driven droplet growth leads to shape instabilities that trigger the division of droplets into two smaller daughter droplets. Chemically active droplets can exhibit cycles of growth and division that resemble the proliferation of living cells, and dividing active droplets could therefore act as a model for prebiotic protocells (Zwicker et al., 2017).

Another example is the Saffman-Taylor, or viscous fingering instability describes the formation of patterns in a morphologically unstable interface between two fluids in a porous medium, such as during drainage through soils. A less viscous fluid is injected to displace a more viscous fluid. In a rectangular configuration the system evolves until a single finger forms. In the radial configuration the pattern grows forming fingers by successive tip-splitting. Research on viscous fingering has been performed on Hele-Shaw cells, where two closely spaced and parallel sheets of glass contain a viscous fluid. In the channel configuration set-up, the less viscous fluid is injected at one end of the channel. In the radial configuration set-up, the less viscous fluid is injected at the center of the cell (Wikipedia.org, 2021).

The Richtmyer-Meshkov instability comes from an impulsively accelerated interface between two materials of different density. Originally studied in fluids, more recent studies investigate material properties of solids. Instability growth rate and resulting profile are dependent on initial shock strength and non-dimensional perturbation. Information from such experiments is used to calibrate and validate numeric model parameters, and the oscillatory shock front in the liquid tamping media can then be used to approximate any viscosity from a transient 1-D analytics (Olles et al., 2021).

The Kelvin-Helmholtz instability occurs when there is velocity shear in a single continuous fluid. It can also occur where there is a velocity difference across the interface between two fluids. One example is when wind blows across a liquid surface creating waves. They are further visible in the atmospheres of planets and moons in form of cloud formations on Earth or the Red Spot on Jupiter, as well as the corona of stars (Wikipedia.org, 2021). Both, the Saffman-Taylor and the Richtmyer-Meshkov methods do not incorporate a form of diffusion into the models, yet the Kelvin-Helmholtz does.

Mathematical models and validations of all of the aforementioned instabilities have been proven and the theories validated.



Figure 26: Viscous fingering shown in Hele-Shaw cells consisting of two parallel sheets of glass and a viscous fluid (Wikipedia.org, 2021).

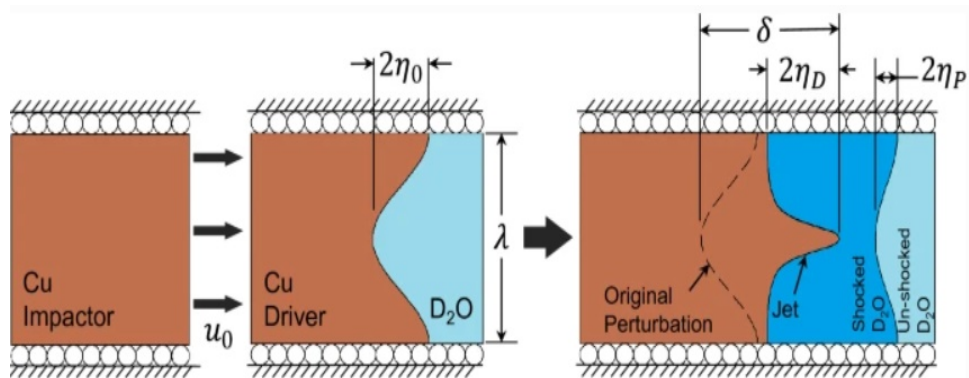


Figure 27: Richtmyer-Meshkov model for an interface between two materials of different densities (Olles et al., 2021).



Figure 28: Dendritic growth in copper from a copper sulfate solution (Matthiesen, S., 2013).

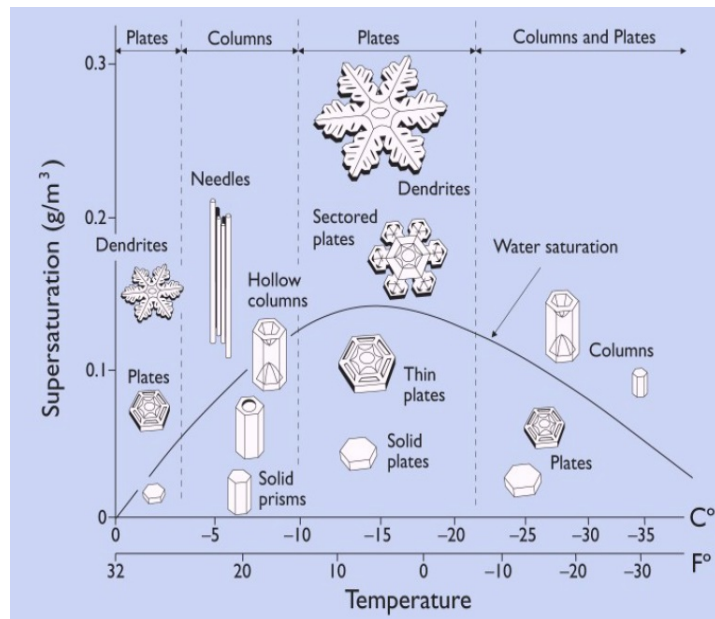


Figure 29: Temperature vs. Supersaturation in the formation of different types of snowflakes, dendrite formation, and crystals (Matthiesen, S., 2013).

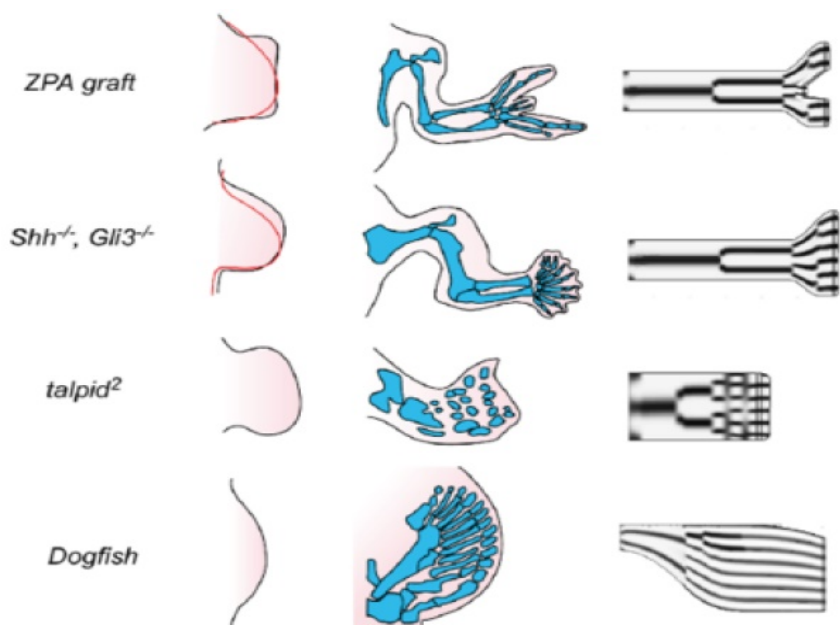


Figure 30: Limb bud expansion in a variety of organisms, showing growth focus at the tip of the limb, where growth in other parts is minimized (wikipedia.org, 2021).

### 3 Sources and References

Deutsch, J. Biophysics Lecture Material, University of California Santa Cruz, 2021

Langer, J. S. (1980). Instabilities and pattern formation in crystal growth\*. Carnegie-Mellon University, Physics Department and Center for the Joining of Materials.

Maini, P. K., Woolley, T. E., Baker, R. E., Gaffney, E. A., Lee, S. S. (2012). Turing's model for biological pattern formation and the robustness problem. *Interface focus*, 2(4), 487–496. <https://doi.org/10.1098/rsfs.2011.0113>

<https://oceanconservancy.org/blog/2019/10/07/octopuses-change-color>

Olles, J.D., Hudspeth, M.C., Tilger, C.F. et al. The Effect of Liquid Tamping Media on the Growth of Richtmyer–Meshkov Instability in Copper. *J. dynamic behavior mater.* (2021). <https://doi.org/10.1007/s40870-021-00305-8>

<https://www.quantamagazine.org/biologists-home-in-on-turing-patterns-20130325>

Sander, Evelyn (2001). Animal Coat Pattern Formation. George Mason University, Department of Mathematical Sciences. 1-26.

[https://www.stephan-matthiesen.de/images/material/0049/MatthiesenOLLPatterns2011\\_06\\_Growth.pdf](https://www.stephan-matthiesen.de/images/material/0049/MatthiesenOLLPatterns2011_06_Growth.pdf)

Turing Patterns to Generate Stripes and Spots. University of the Pacific, 3 Jan. 2021, <https://bio.libretexts.org/@go/page/148>

<https://en.wikipedia.org/wiki/Kelvin-Helmholtz-instability>

<https://en.wikipedia.org/wiki/Saffman-Taylor-instability>

Zwicker, D. et al. Growth and division of active droplets provides a model for protocells. *Nat. Phys.* 13, 408–413 (2017)